Similarities in the electrical conduction processes in hydrogenated amorphous silicon oxynitride and silicon nitride

2003 J. Phys.: Condens. Matter 15 2197

(http://iopscience.iop.org/0953-8984/15/13/305)

INSTITUTE OF PHYSICS PUBLISHING JOURNAL OF PHYSICS: CONDENSED MATTER

J. Phys.: Condens. Matter **15** (2003) 2197–2205 PII: S0953-8984(03)53306-9

Similarities in the electrical conduction processes in hydrogenated amorphous silicon oxynitride and silicon nitride

Hiromitsu Kato[1], **Hidefumi Sato**[1], **Yoshimichi Ohki**[1,4], **Kwang Soo Seol**[2,4] **and Takashi Noma**[3,4]

[1] Department of Electrical, Electronic and Computer Engineering, Waseda University, Shinjuku-ku 169-8555, Japan
[2] RIKEN (The Institute of Physical and Chemical Research), Wako 351-0198, Japan
[3] Engineering Department 1, System-LSI Division, Sanyo Electric Co. Ltd, Oizumi-Machi 370-0596, Japan
[4] Advanced Research Institute for Science and Engineering, Waseda University, Shinjuku-ku 169-8555, Japan

E-mail: hiromitsu_kato@asagi.waseda.jp

Received 11 September 2002
Published 24 March 2003
Online at stacks.iop.org/JPhysCM/15/2197

Abstract

Electrical conduction at high fields was examined in a series of hydrogenated amorphous silicon oxynitride and silicon nitride films with different nitrogen contents deposited by plasma-enhanced chemical vapour deposition. It was shown that the conduction is attributable to the Poole–Frenkel (PF) emission in the two materials. The energy depths of the PF sites and the dependences on the sample's chemical composition are quite similar for the two samples. It is considered that the PF sites in the two materials are identical.

1. Introduction

Hydrogenated amorphous silicon oxynitride (a-SiO_xN_y:H) and silicon nitride (a-SiN_z:H) films deposited using plasma-enhanced chemical vapour deposition (PECVD) have a wide range of applications ranging from use as insulating dielectrics in thin-film transistors [1–3] to use as more conductive films for light-emitting devices [4–6]. They are also attracting attention since they have potentiality for use in solar cells [7, 8], optical fibres [9] and waveguides [10, 11]. Depending on how they are deposited and operated, however, thin-film devices made with a-SiO_xN_y:H and a-SiN_z:H contain various quantities of localized states due to structural disorder and defects, many of which are charged and cause an increase in their conductivities. In view of this, much effort has been devoted to clarifying the mechanism of the conduction in these materials [12–15].

Authors have been investigating these materials mainly through analyses of their photoluminescence characteristics and have already reported that they possess localized band-tail states associated with Si–N bonds [16–20]. However, the effects of these states on the electrical conduction remain to be studied. In this paper, we investigate the electrical conduction processes in these materials at high fields.

2. Experimental procedures

The a-SiO_xN_y:H films were deposited using a dual-frequency PECVD system. A mixture of SiH_4, N_2O and N_2 gases was excited in a parallel-plate reactor where a radio-frequency (rf) power of 13.56 MHz was supplied with a maximum power of 0.54 kW. At the same time, a lower-frequency power of 400 kHz was also supplied with a maximum power of 0.38 kW to reduce the structural stress of the deposited film. Films of three types with different atomic ratios were prepared by changing the flow ratio of SiH_4 to the sum of the other two gases. The films were deposited onto a p-type (100) silicon monocrystal substrate set on a stage whose temperature was kept constant at 400 °C. Films of a-SiN_z:H of three types were similarly deposited using a mixture of SiH_4, N_2 and NH_3 gases. The elemental compositions of Si, O and N were estimated through x-ray photoelectron spectroscopy (XPS, JEOL JPS-90MX). The refractive index was measured by ellipsometry (ULVAC ESM-1) with a He–Ne laser at a wavelength of 632.8 nm.

The electrical properties were examined by measuring the conduction current using a high-resistance meter (Advantest R8340) and the capacitance using a high-frequency C–V meter (Sanwa Mega Bytek MI-494) for the sample having a metal–insulator–semiconductor (MIS) structure consisting of the lower silicon substrate, the film and an evaporated gold upper electrode with an effective area of 7.9×10^{-3} cm^2. The conduction current was measured at 0, 25, 50, 75, 100 and 125 °C by applying a negative dc voltage to the gold electrode while changing its value from 0 to 150 V in a stepwise manner with a step of 0.15 V. The relative permittivity was calculated from the capacitance of the accumulation layer measured at room temperature.

3. Results and discussion

The elemental compositions of all the a-SiO_xN_y:H and a-SiN_z:H films examined have been determined by XPS, as shown in table 1. For a-SiO_xN_y:H films (samples A, B and C), the nitrogen and the silicon contents decrease with decrease in the gas flow ratio of SiH_4 to the sum of the other two gases [$SiH_4/(N_2O + N_2)$]. The silicon content decreases for a-SiN_z:H films (samples D, E and F) with a similar decrease in the gas flow ratio of SiH_4 to the other two gases. If the apparent chemical composition of a-SiO_xN_y:H is expressed by the relation $(1/2)x(SiO_2) + (1/4)y(Si_3N_4)$, the value $(1/2)x + (3/4)y$ becomes unity. The value becomes less than unity if surplus silicon is present, as compared to the above equation. That is, the value can be regarded as an abundance ratio of atoms other than silicon ones to silicon atoms. For the sake of simplicity, this value is called the abundance ratio. The ratio approaches unity in the order of samples A, B, C, indicating that silicon is the most abundant in sample A and the least abundant in sample C. For a-SiN_z:H, the value $(3/4)z$ is the abundance ratio, which indicates that samples D and F are the most and the least abundant in silicon, respectively.

Figure 1 shows the conduction current density J measured at room temperature as a function of the electric field intensity E obtained for all the samples. The following three systematic trends can be observed as the abundance ratio increases regardless of whether the sample is a-SiO_xN_y:H or a-SiN_z:H.

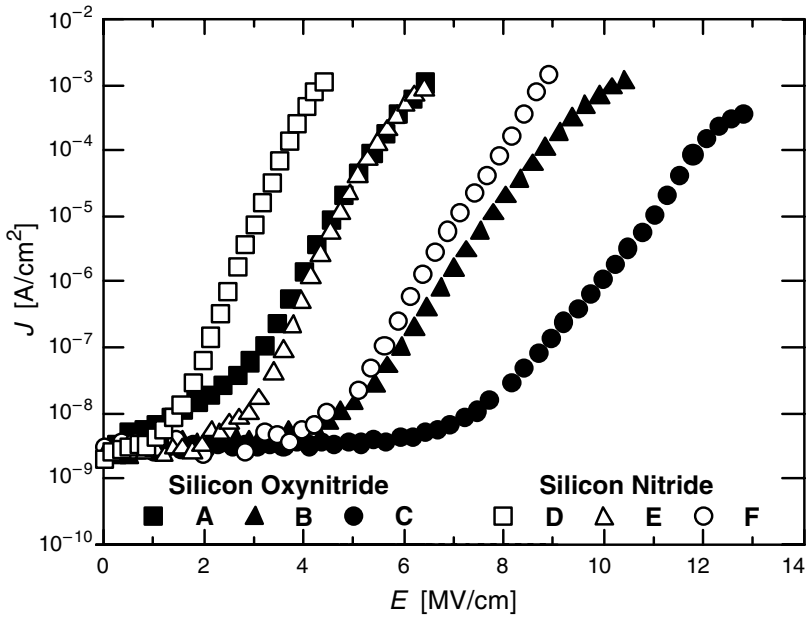

Figure 1. The relation between the electric field intensity E and the conduction current density J measured in samples A–F at room temperature.

Table 1. Elemental compositions, gas flow rates, abundance ratios of atoms other than silicon ones to silicon atoms and refractive indices of the a-SiO_xN_y:H and a-SiN_z:H films tested.

Sample	Gas flow ratio	Atomic %			Abundance ratio	Refractive index
Silicon oxynitride	$SiH_4/(N_2O + N_2)$	Si	O	N	$\{(1/2)O + (3/4)N\}/Si$	
A	3.7×10^{-2}	38	53	9.6	0.89	1.68
B	3.0×10^{-2}	37	56	7.7	0.91	1.63
C	2.4×10^{-2}	35	57	7.0	0.96	1.57
Silicon nitride	$SiH_4/(NH_3 + N_2)$	Si	—	N	$\{(3/4)N\}/Si$	
D	1.2×10^{-1}	52	—	47	0.68	2.08
E	8.6×10^{-2}	50	—	49	0.73	1.99
F	5.1×10^{-2}	44	—	55	0.95	1.91

(i) The high-field end of each curve indicating the point of dielectric breakdown shifts to a higher electric field.
(ii) Each curve can be divided into two regions. The onset of the high-field region shifts to a higher electric field.
(iii) The slope of each curve in the high-field region decreases.

Sample C or F with the highest abundance ratio exhibits the highest breakdown field, the smallest slope and the lowest leakage current if compared at the same electric field, while sample A or D with the lowest abundance ratio exhibits the lowest breakdown field, the steepest slope and the highest leakage current.

Focusing on the high-field region, the conduction process is discussed. The Poole–Frenkel (PF) emission (equation (1)) and the Fowler–Nordheim (FN) tunnelling (equation (2))

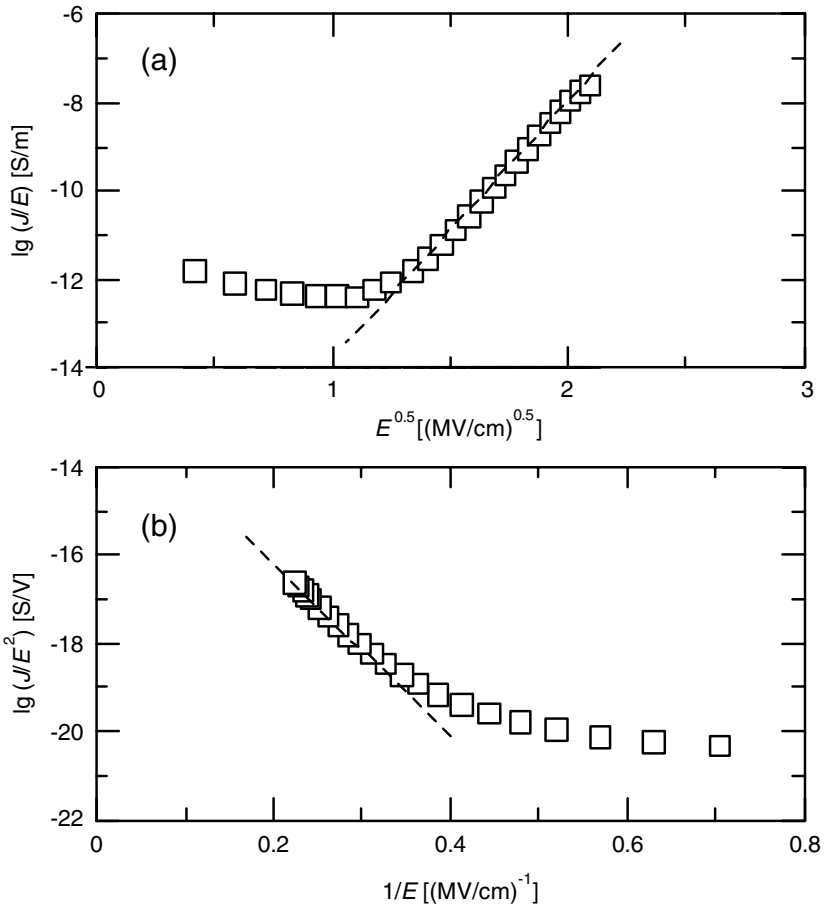

Figure 2. A PF plot (a) and a FN plot (b) obtained for sample D. The broken straight line indicates either the PF or the FN relation, obtained by least-squares fitting to the data at high fields.

are frequently observed in silicon nitride at high fields [12, 13]:

$$J_{PF} = C_{PF} E \exp\left[-\frac{1}{kT}\left(\phi_{PF} - \sqrt{\frac{q^3 E}{\pi \varepsilon_0 \varepsilon_{in}}}\right)\right], \tag{1}$$

$$J_{FN} = \frac{q^3 E^2}{8\pi h \phi_{FN}} \exp\left[-\frac{8\pi\sqrt{2m^*}\phi_{FN}^{3/2}}{3qhE}\right]. \tag{2}$$

Here C_{PF} is a constant with the dimension of conductivity, q is the electronic charge, k_B is the Boltzmann constant, T is the absolute temperature, ϕ_{PF} is the energy depth of the PF sites, ε_0 is the permittivity of free space, ε_{in} is the permittivity of the insulating layer, h is the Planck constant, ϕ_{FN} is the height of the barrier between the Fermi level of the metal and the conduction band of the insulating layer and m^* is the effective mass of the electron. The PF current density J_{PF} is bulk limited, i.e., the current is controlled by the defect states present below the conduction band and above the valence band. The FN current density J_{FN} occurs as a result of carrier tunnelling through a triangular potential barrier.

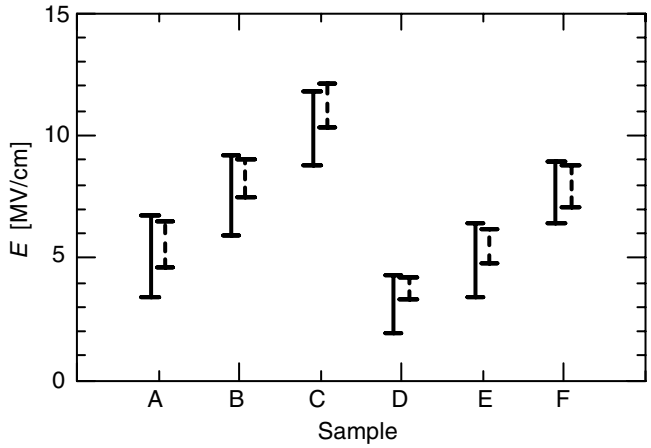

Figure 3. Regions of electric field intensities in which the J–E characteristics agree with the PF relation (solid lines) or with the FN relation (broken lines), obtained for samples A–F.

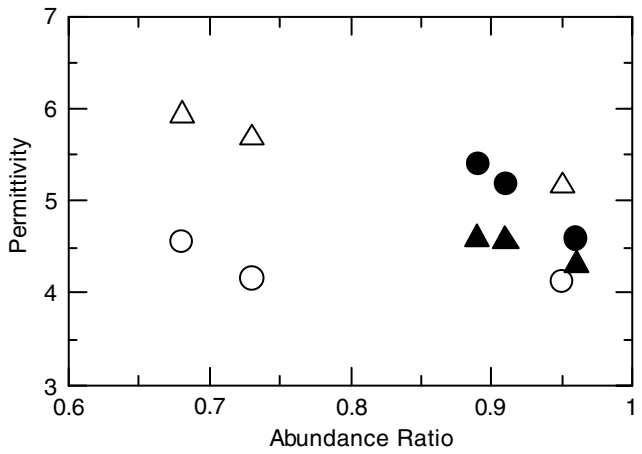

Figure 4. Permittivities calculated from the PF plots (circles) and those calculated from the capacitance values of the accumulation layers (triangles). Solid and open symbols show the data obtained for a-SiO_xN_y:H and a-SiN_z:H, respectively.

Figure 2(a) shows a PF plot drawn based on the J–E relation observed for sample D, while figure 2(b) shows its FN plot. Similar PF and FN plots were drawn for all the J–E curves shown in figure 1, and the field regions where the PF or the FN relation governs the conduction current were estimated by drawing straight lines using the least-squares method as shown in figure 2. Figure 3 compares such estimated regions. It is clear that the high-field conduction is more governed by the PF process regardless of whether the sample is a-SiO_xN_y:H or a-SiN_z:H.

The relative permittivity of each film was calculated using equation (1) from the slope of the PF curve, e.g. the slope of the broken line shown in figure 2(a) in the case of sample D. Figure 4 shows the relative permittivity as a function of the abundance ratio. The relative permittivity values calculated from the capacitance values of the accumulation layers are also shown in figure 4. The permittivity values calculated in both ways decrease with increase in the abundance ratio, consistently with the refractive index shown in table 1. Although the

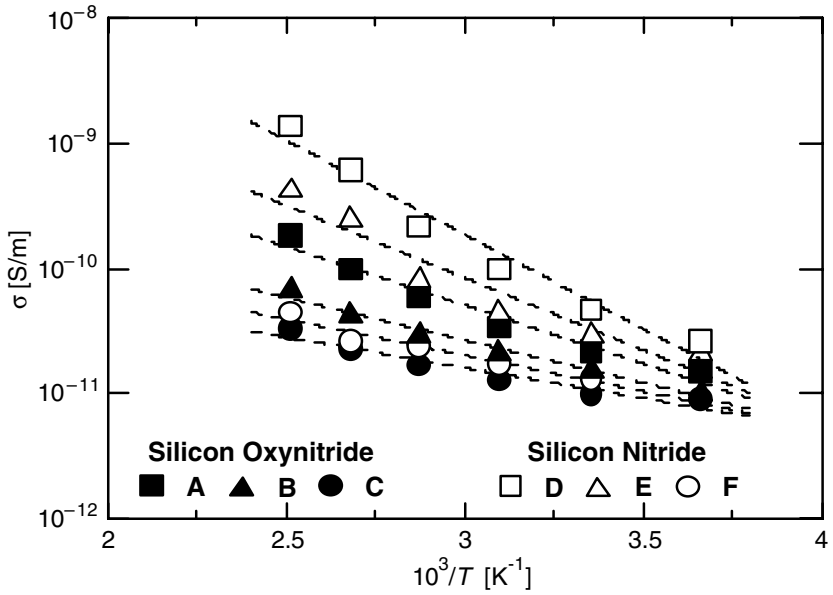

Figure 5. Arrhenius plots of conductivities obtained for samples A–F. The broken lines are obtained by least-squares exponential fitting to the data.

permittivity value calculated from the slope and the one calculated from the capacitance do not agree with each other, their dependences on the abundance ratio are similar.

Figure 5 shows the Arrhenius plot of the conductivity σ. Here, σ was obtained according to the following procedures. As shown in figure 1, the J–E curve strongly depends on the sample's abundance ratio. It is reasonable to adopt the conductivity value around the mid-point of the J–E curve in the high-field region. On this basis, the values of the electric field where the current density measured at 25 °C became 1×10^{-6} A cm^{-2} were read from figure 1. These constant values of the electric field, such as 9.9 MV cm^{-1} for sample C and 2.6 MV cm^{-1} for sample D, were used to calculate σ, not only at 25 °C but also at the other temperatures. Note that the slopes of the Arrhenius plots do not vary if we change the starting value of the electric field within the region where the PF relation holds. The logarithmic conductivity shown in figure 5 has a PF-type temperature dependence, while the FN current theoretically does not depend on the temperature. Therefore, the above-mentioned facts indicate that the high-field conduction is due to the PF emission.

Figure 6 shows the energy depth ϕ_{PF} as a function of the abundance ratio estimated from the Arrhenius plot shown in figure 5. The depth ϕ_{PF} increases monotonically from 0.85 to 1.21 eV with increase in the abundance ratio. Furthermore, the large value of ϕ_{PF} should be responsible for the low conduction current and high breakdown field in the samples with high abundance ratios, the characteristics clearly shown in figure 1.

The energy depth ϕ_{PF} is an important parameter in the PF process. It is interesting to see how ϕ_{PF} governs the PF processes in the two different but similar materials a-SiO_xN_y:H and a-SiN_z:H. The vertical bars in figure 7 represent the maximum and minimum field intensities in the regions where the conduction current in each sample obeys the PF relation. A striking similarity between the two materials is illustrated, which indicates that the PF sites in the present two kinds of sample have the same origin regardless of the presence of oxygen. This is consistent with our previous conclusion obtained from photoluminescence analyses that

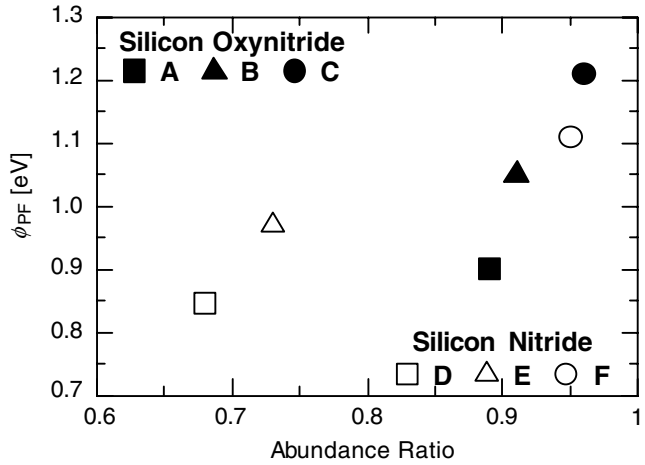

Figure 6. Change in the energy depth of the PF sites ϕ_{PF} as a function of the abundance ratio. Solid and open circles show the data obtained for a-SiO_xN_y:H and a-SiN_z:H, respectively.

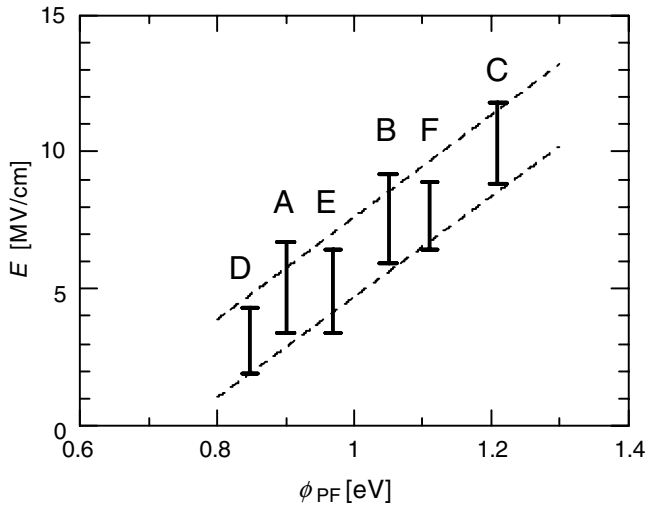

Figure 7. Changes in the electric field regions in which the J–E characteristics agree with the PF relations, as a function of the energy depth ϕ_{PF}. Each broken straight line indicates each end of the region, obtained by least-squares fitting. Letters A–F represent samples A–F.

a-SiO_xN_y:H and a-SiN_z:H possess similar localized band-tail states associated with Si–N bonds [17, 20]. Moreover, the width of these localized states has been reported to become broader with increase in the abundance ratio, indicating that the carriers are localized in deeper states [20, 21]. This is consistent with the present result shown in figure 6. Therefore, it is concluded that the electrical conduction in a-SiO_xN_y:H and a-SiN_z:H at high fields is governed by the PF process through the localized states associated with Si–N bonds located either below the conduction band or above the valence band.

A few words are now added about the band-tail states. Although the present six films contain hydrogen, that the band-tail states have no relation to hydrogen has already been

clarified using silicon oxynitride films prepared by rapid thermal nitridation of silicon dioxide in a hydrogen-free NO ambience [18]. Furthermore, one might consider that it would be reasonable to use the N/Si ratio rather than the abundance ratio, if the PF sites are associated with Si–N bonds. For a-SiN_z:H, the two ratios have exactly the same meaning, but this is not the case for a-SiO_xN_y:H. In a-SiO_xN_y:H, there are Si–N bonds and Si–O bonds. The N/Si ratio takes all the Si atoms into account, while only those bonded with N atoms are presumed important. Since it is impossible to estimate the number of Si atoms bonded with N, the sole parameter that we can use is the abundance ratio. As mentioned above, we have already confirmed that the photoluminescence can also be understood systematically for the present a-SiO_xN_y:H and a-SiN_z:H films using the abundance ratio as a common parameter [20]. Finally, the validity of extending the present conclusion to similar films synthesized by other fabrication methods is unclear. Although we have found that the photoluminescence mechanism is the same for 5.8 nm thick silicon oxynitride films fabricated by rapid thermal nitridation of silicon dioxide, for 75 nm thick a-SiN_z:H films fabricated by low-pressure CVD and for 100 nm thick a-SiO_xN_y:H films fabricated by PECVD [17, 18], the conduction process seems to be much more highly dependent on the film thickness.

4. Conclusions

We have examined the electrical conduction mechanism in a-SiO_xN_y:H and a-SiN_z:H, and have found that the current at high fields is governed by the PF emission in both materials. From the similarity as regards many aspects of the conduction process, it is considered that the carriers in the two materials are transported similarly through the PF sites associated with Si–N bonds.

Acknowledgments

H Kato is a Research Fellow of the Japan Society for the Promotion of Science. This work was partly supported by Grants-in-Aid from the Japan Society for the Promotion of Science (JSPS) for JSPS Fellows (No 1205733), for Scientific Research (B) (No 12450132) and for Encouragement of Young Scientists (No 12750307). A High-Tech Research Grant from the Ministry of Education, Culture, Sports, Science and Technology of Japan is also appreciated.

References

[1] Murata M, Yamauchi K, Kojima H, Yokoyama A, Inoue T and Iwamori T 1993 *J. Electrochem. Soc.* **140** 2346
[2] Desbiens E, Dolbec R and El Khakani M A 2002 *J. Vac. Sci. Technol.* A **20** 1157
[3] Fukuda H, Arakawa T and Ohno S 1990 *Electron. Lett.* **26** 1505
[4] Kanemitsu Y, Futagi T, Matsumoto T and Mimura H 1994 *Phys. Rev.* B **49** 14723
[5] Kato H, Masuzawa A, Sato H, Noma T, Seol K S, Fujimaki M and Ohki Y 2001 *J. Appl. Phys.* **90** 2216
[6] Prokes S M and Carlos W E 1995 *J. Appl. Phys.* **78** 2671
[7] Boehme C and Lucovsky G 2000 *J. Appl. Phys.* **88** 6055
[8] King R R, Sinton R A and Swanson R M 1990 *IEEE Trans. Electron Devices* **ED-37** 365
[9] Dianov E M, Golant K M, Khrapko R R, Kurkov A S and Tomashuk A L 1995 *J. Lightwave Technol.* **13** 1471
[10] Kato H, Fujimaki M, Noma T and Ohki Y 2002 *J. Appl. Phys.* **91** 6350
[11] Hoffmann M, Kopka P and Voges E 1997 *IEEE Photonics Technol. Lett.* **9** 1238
[12] Tao M, Park D, Mohammed S N, Li D, Botchkerav A E and Morkoc H 1996 *Phil. Mag.* B **73** 723
[13] Kennedy G P, Buiu O and Taylor S 1999 *J. Appl. Phys.* **85** 3319

[14] Manzini S and Volonte F 1985 *J. Appl. Phys.* **58** 4300
[15] Boher P, Renaud M, Vanljzendoorn L J, Barrier J and Hily Y 1988 *J. Appl. Phys.* **63** 1464
[16] Kato H, Masuzawa A, Noma T, Seol K S and Ohki Y 2001 *J. Phys.: Condens. Matter* **13** 6541
[17] Noma T, Seol K S, Fujimaki M, Kato H, Watanabe T and Ohki Y 2000 *Japan. J. Appl. Phys.* **39** 6587
[18] Noma T, Seol K S, Kato H, Fujimaki M and Ohki Y 2001 *Appl. Phys. Lett.* **79** 1995
[19] Seol K S, Watanabe T, Fujimaki M, Kato H, Ohki Y and Takiyama M 2000 *Phys. Rev.* B **62** 1532
[20] Kato H, Kashio N, Ohki Y, Seol K S and Noma T 2003 *J. Appl. Phys.* **93** 239
[21] Searle T M and Jackson W A 1989 *Phil. Mag.* B **60** 237